ACS APPLIED MATERIALS & INTERFACES

Research Article

www.acsami.org

Novel Poly(tetramethylene ether)glycol and Poly(ε-caprolactone) Based Dynamic Network via Quadruple Hydrogen Bonding with Triple-Shape Effect and Self-Healing Capacity

Min Wei, Miqin Zhan, Dongqin Yu, Hui Xie, Manjie He, Keke Yang,* and Yuzhong Wang

Center for Degradable and Flame-Retardant Polymeric Materials (ERCEPM-MoE), National Engineering Laboratory of Eco-Friendly Polymeric Materials (Sichuan), State Key Laboratory of Polymer Materials Engineering, Sichuan University, Chengdu, Sichuan 610064, China

ABSTRACT: A novel dynamic network was successfully prepared via self-complementary quadruple hydrogen bonding through Upy-telechelic poly(tetremethylene ether) glycol (PTMEG) and four-arm star-shaped poly(ε-caprolactone) (^{4}PCL) precursors. The structure and the dynamic feature were identified by FT-IR and ^{1}H NMR. The differential scanning calorimetry (DSC) analysis indicated that the crystalline PCL and PTMEG segments show a separated melting peak, and the aggregation of Upy dimer was also observed. The dynamic mechanical analyzer (DMA) test reveals that the storage modulus of the network drops evidently across the thermal transition. These characteristics of the network ensure that it exhibits a triple-shape effect, and the composition of the network influences the performance of shape memory effect. The variation of the fixing ratio of the network in each deformation step is quite according to the crystallinity of the dominant segment. The reversibility of the quadruple hydrogen bonding between Upy dimer endues the network with self-healing capacity, and the damage and healing test of the network revealed that increasing the content of the PTMEG segment will be of benefit to self-healing performance.

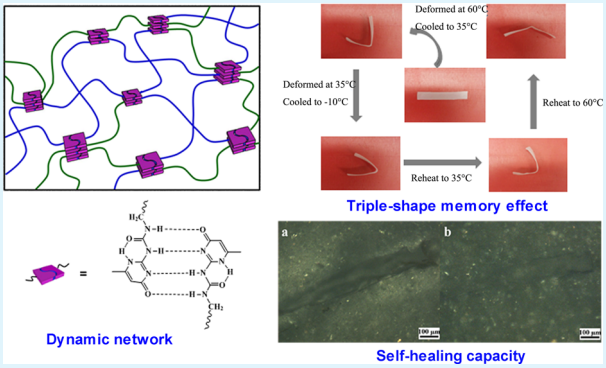

KEYWORDS: *dynamic network, quadruple hydrogen bonding, triple-shape effect, self-healing*

INTRODUCTION

As a promising intelligent material, shape memory polymers (SMPs) have the capability of changing the shape in a predefined way for responding to different external stimuli, like heat, light, chemicals (moisture, solvent, pH, or other chemicals), etc.[1−8] This stimuli-sensitive nature of SMP enables it to be applicable in varying fields such as sensors,[9] actuators,[10] smart devices,[11−13] and biomedical engineering.[14] The most attractive advantage of SMPs is that one can easily tailor their structural parameters of the molecular architecture to fulfill the increasing demands of the specific application. Thus, the smart SMPs with multishape memory effect,[15,16] multiresponsibility,[17,18] and multifunctionality[19] have drawn much attention of the researchers.

Among the various stimuli, thermally induced SMPs have been intensively investigated for easy design and implementation. From the view of a basic working mechanism, the thermally induced SMPs actually can be classified into three categories, namely, the dual-phase transition mechanism, dual-component mechanism, and partial-transition mechanism.[14,20] Within the dual-phase transition mechanism, when a glassy polymer is heated to above its glass transition temperature (T_g), it is easy to be deformed since it is in a rubbery state. Upon cooling down to T_g, the motion of the polymer chains is frozen even after the removal of the applied constraint. When the polymer is heated into a rubbery state again, shape recovery can be observed. Within the dual-component mechanism, a SMP commonly contains a molecular switch component and an elastic component. The molecular switch plays the role of fixing the temporary shape and responding to the stimulus while the elastic component determines the permanent shape. The polymers, which exhibit reversible thermal transition, may be utilized as molecular switch components, and their glass transition temperature (T_g), melting temperature (T_m), or liquid crystalline clearing transition (T_{cl}) may act as the transition temperature (T_{trans}). As we know, various SMPs are developed from this mechanism. Recently, the partial-transition mechanism has been mentioned, and this mechanism may work along or together with other two mechanisms. Besides, SME has also been found in melting glue, such as thermoplastic polyurethanes (TPUs) with low melt-flow index and non-cross-linking.[21]

If the SMPs can only memorize one temporary shape in a shape memory cycle, then they are dual-shape materials (DSM),[22−24] and generally, they have a single T_{trans} in the switch domain. Recently, the multishape memory polymers

Received: November 1, 2014
Accepted: January 5, 2015
Published: January 5, 2015

 © 2015 American Chemical Society

DOI: 10.1021/am507575z
ACS Appl. Mater. Interfaces 2015, 7, 2585−2596

(MSMPs), which can change and recover from multiple shapes, were explored to meet the increasing requirements.[25−30] Xie developed a new strategy to design the MSMPs to rely on a single broad thermal transition. He reported a perfluorosulfonic acid iomer (PFSA)[31] and V-shaped gradient copolymer of styrene and methyl acrylate,[32] which has only one broad T_g, exhibiting dual-, triple-, and even quadruple-shape memory effects. Peng and Ding and co-workers reported PMMA/PEG semi-IPNs with quadruple-shape memory effect by using two gradients T_g from a broadened glass transition and a T_m of PEG as three T_{trans} values.[33] Among the varying MSPs, triple-shape memory polymers (TSMPs), which can memorize two temporary shapes in one shape memory cycle, are extensively explored.[34,35] A simple strategy is to combine two switching phases in the networks. Bellin and his co-workers have demonstrated the triple-shape memory effect in systems containing two switching phases, the T_m of the PEG crystal and the T_g of the semi-IPNs.[25] Luo and his co-workers have also demonstrated a system of composites capable of demonstrating the triple-shape memory effect.[28] Wang and his co-workers prepared a polymer network based on ethyl cellulose (EC) grafted with two different molecular weights of poly(ε-caprolactone) (PCL), which well exhibit triple-shape memory effects.[29] Zhou and his co-workers reported triple-shape memory polyurethane networks obtained via simple photo-cross-linking of cinnamon groups which include both a T_m-type segment and a T_g-type segment.[35] In our previous work, we design a series of TSMPs by introducing crystalline aliphatic polyesters (PPDO and PCL) with aliphatic polyethers (PEG and poly(tetremethylene ether) glycol (PTMEG)) into a co-network[36,37] or interpenetrating networks.[38]

To achieve MSMPs, more attention is focused on the design of the molecular switch; actually, the architecture of the netpoint is also very important for the shape-memory effect. In the system we mentioned above, the most commonly used netpoints are physical cross-linking based on crystalline or chemical cross-linked networks especially by covalent bonds. Although the covalently cross-linked polymer networks exhibit excellent memory ability, they are dramatically limited in many fields of application since they are not generally reconfigurable, recyclable, and reprocessable. Recently, the dynamic networks have drawn tremendous attention of researchers for their triggerable and reversible nature,[39] which may be constructed by the dynamic covalent bond and dynamic noncovalent bond. The application of the dynamic covalent bond in the design of SMPs architecture has been involved in the last several years. Raquez and his co-workers prepared a dual-shape PCL-based network through Diels−Alder reactions by reactive extrusion, which shows one-way and two-way shape-memory properties.[40] Ninh and Bettinger reported dual-shape biodegradable polyester networks via Diels−Alder coupling.[41] In our previous work, a triple-shape PPDO−PTMEG co-network with self-healing effect was developed.[36]

With the rapid development of supramolecular chemistry, the dynamic network based on noncovalent interactions has been widely used in the smart materials including shape-memory materials.[42] Among the varying noncovalent interactions, such as hydrogen bonding, electrostatic, metal ion coordination, and $\pi-\pi$ interactions, hydrogen bonding is a favorable choice to structure a reversible polymer network.[43] Weck and his co-workers developed a series of polymer networks based on the complementary hydrogen bond, which shows multiresponsibility and tunable properties.[44] Meijer et al. first demonstrated the unique ability of self-complementary arrays of hydrogen bonding in the formation of supramolecular polymers, specifically utilizing 2-ureido-4[1H]-pyrimidone (UPy) units.[45,46] The high dimerization constant (6×10^7 M^{-1} in chloroform)[47,48] and predictable tautomerism make it possible to obtain supramolecular polymers materials with a high degree of polymerization.[49,50] Likewise, the shape-memory polymer networks may be constructed by incorporating the Upy motifs to polymer chains in both the pendent side group[30,51] and main chain.[52]

Actually, taking advantage of reversible characteristics of dynamic interactions to develop self-healing materials becomes the fascinating challenge of the materials scientist.[53−56] A large number of self-healing polymers are created on the basis of hydrogen bonding,[57−59] metal−ligand coordination, and $\pi-\pi$ interactions, which can be induced by heat treatment or irradiation.[55,56] The hydrogen bonding between the Upy group has been identified by Guan and co-workers[58] as a good dynamic bond to trigger the self-healing effect, so we try to combine the advantage of the Upy group in the construction of the shape-memory dynamic network as well as the self-healing material.

In the present work, we try to produce a novel dynamic network via self-complementary hydrogen bonding from Upy-telechelic poly(tetremethylene ether) glycol (PTMEG) and four-arm star-shaped poly(ε-caprolactone) (^{4}PCL) precursors. Here, crystalline PTMEG and PCL segments with a separated melting temperature act as two switching domains, ensuring the material exhibits a triple-shape effect. The dimerization of Upy groups forms the netpoints for TSPs, and the aggregation of Upy dimers should enhance the netpoints further. More important, the reversibility of the dynamic networks endows its reprocessability and self-healing feature.

EXPERIMENTS AND METHODS

Materials. The ε-caprolactone was purchased from Alfa Aesar (UK). It was dried over CaH_2 and distilled under reduced pressure before use. Poly(tetremethylene ether)glycol (AR grade, M_n =2900 g mol^{-1}), 1,6-hexamethylene diisocyanate (HDI) (AR grade), stannous octoate ($SnOct_2$) (≥95%), and guanidine carbonate (AR grade) were purchased from Sigma-Aldrich (USA) and used without further purification. Before use, the $SnOct_2$ was fist diluted with dry toluene and stored in a glass volumetric flask under argon. Pentaerythritol (PTOL) (Sinopharm Chemical Reagent Co.) was sublimated under reduced pressure. Dibutyltin dilaurate (DBTL) was purchased from Sinopharm Chemical Reagent Co. and used as received. Chloroform was supplied by Kelong Reagent Corp. (Chengdu, China). It was refluxed and dehydrated by phosphorus pentoxide for 24 h and distilled before used. Ethyl acetoacetate (EAA) was supplied by Bodi Chemical Corp. (Tianjin, China). It was dehydrated by magnesium sulfate for 48 h and distilled under reduced pressure before use. All other reagents and solvents were reagent grade and used as received.

Preparation of 1-(6-Isocyanate)-3-(6-methyl-4-oxo-1,4-dihydropyrimidin-2-yl) Urea (UPy). A suspension of guanidine (added as guanidine carbonate, 14.90 g, 0.08 mol) and EAA (23.34 mL, 0.18 mol) in dry ethanol (180 mL) was refluxed for 12 h, giving a white mixture. The white mixture was filtered on a Büchner funnel, and a white solid appeared; then, it was washed with dry ethanol, deionized water, and acetone in sequence. The white solid was further dried in a vacuum oven overnight to yield 6-methylisocytosine (MIC), **1**. Then, MIC (5.82 g, 0.05 mol) and HDI (54.4 g, 0.32 mol) were added into a round-bottom flask under a nitrogen atmosphere and refluxed at 100 °C for 12 h. Next, the mixture was added to petroleum ether (200 mL) to give a white precipitate. The white precipitate was filtered on a Büchner funnel, washed with petroleum ether, and dried in a 50 °C vacuum oven for 5 h to give UPy, **2**.

DOI: 10.1021/am507575z
ACS Appl. Mater. Interfaces 2015, 7, 2585−2596

Scheme 1. Synthetic Routes of (A) UPy, (B) ^{4}PCL-U, and (C) PTMEG-U

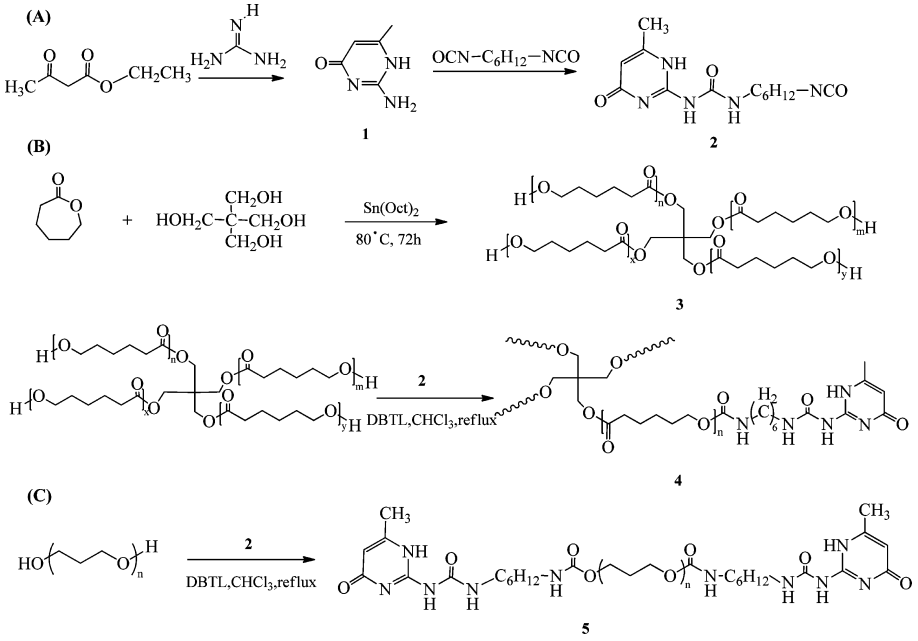

Preparation of UPy-Functionalized Four-Arm Star-Shaped PCL (^{4}PCL-U). ^{4}PCL-U was prepared by two steps: In first step, ^{4}PCL was prepared by typical bulk ring-opening polymerization of ε-caprolactone using pentaerythritol (PTOL) as initiator and $SnOct_2$ as catalyst. In detail, PTOL (1.75 g, 12.88 mmol) was put into a 100 mL round flask, which was under vacuum for 3 h to exhaust residual water. After that, the flask was immersed into an oil bath at 120 °C. Then, ε-caprolactone (50 mL, 451.2 mmol) was injected into the flask via a syringe with vigorous stirring for about 5 min. Afterward, $SnOct_2$ (1.80 mL, 0.90 mmol) was added into the mixture, and the mixture was kept stirring for 24 h under nitrogen to get a crude product; then, it was purified by precipitation of a chloroform solution in cold ether and dried in a 40 °C vacuum oven for 24 h to give ^{4}PCL, **3**. In the second step, ^{4}PCL-U was obtained by terminating Upy groups on each arm of ^{4}PCL. In detail, a predetermined amount of UPy (1.92 g, 6.5 mmol) and DBTL was added to the chloroform solution of ^{4}PCL (10 g, 2.17 mmol). The mixture was refluxed at 75 °C under a nitrogen atmosphere for 12 h, resulting in an apparent and viscous liquid. Then, the mixture was injected into a horizontal Teflon dish in a glass autoclave to evaporate the solvent under the protection of a nitrogen stream for 48 h. The resultant film was transferred into a drying oven for 24 h at 50 °C to give UPy-functionalized ^{4}PCL (^{4}PCL-U), **4**.

Preparation of UPy-Functionalized PTMEG (PTMEG-U). The synthetic procedure of PTMEG-U (**5**) was similar to ^{4}PCL-U except the prepoymer change to PTMEG.

Preparation of PCL−PTMEG Network Based on Quadruple Hydrogen Bonding. PCL−PTMEG networks with different contents were prepared by coupling ^{4}PCL-U (**4**) and PTMEG-U (**5**) in chloroform. First, **4** and **5** were mixed in a reaction vessel and dried under vacuum for 3 h to complete dehydration. Then, chloroform was injected into the reaction vessel as the solvent with a nitrogen stream, and the vessel was heated to 70 °C. After 12 h, the mixture was injected into a horizontal Teflon dish in a glass autoclave to evaporate the solvent under the protection of a nitrogen stream; then, the networks were transferred into a drying oven at 50 °C for 2 days. The composition of the networks was adjusted by varying the feed ratio of ^{4}PCL-U (**4**) and PTMEG-U (**5**). The relevant information on all samples synthesized in this work is listed in Table 2. All samples were recorded as PCL_x−$PTMEG_y$, where the subscripts x and y are the mass fractions of **4** and **5**, respectively.

Characterization Methods. ^{1}H NMR spectra were recorded with Bruker AV400 spectrometers (Bruker, Germany) at 400 MHz in $CDCl_3$ and DMSO-d_6, using tetramethylsilane as an internal reference. FT-IR was recorded on a Nicolet MX-1IR spectrometer over the range of 600−4000 cm^{-1} with a 2 cm^{-1} resolution and 50 scans. Gel permeation chromatography (GPC) was performed on a Waters 1515-717-2414 apparatus equipped with a refractive index detector, using monodispersed polystyrene standards to get a calibration curve. The elution solvent was chloroform at a flow rate of 1.0 mL min^{-1} at 30 °C, and sample concentration was about 2.5 mg mL^{-1}. Thermal properties of polymers were determined by differential scanning calorimetry (DSC) analysis, which was carried out with a TA Instrument DSC-Q200 under a steady flow of ultrahigh purity nitrogen. Samples were heated to 100 °C quickly, maintained for 3 min to erase the thermal history, and then cooled down at 5 °C min^{-1} to −50 °C. Subsequently, the samples were heated again to 100 °C at the same rate. The data presented were determined from the cooling curve and the second heating curve. Thermomechanical properties of the samples were tested with a dynamic mechanical analyzer (DMA Q800, TA Instruments, USA) using a multifrequence strain mode at a heating rate of 3 °C min^{-1} from −70 to 80 °C at a frequency of 1 Hz.

Swelling Ratio and Gel Content of the PTMEG−PCL Network. PTMEG−PCL network samples were cut into small slices, swelled, and extracted by chloroform for 2 h. The mass of the unextracted sample (m_0) and the dried extracted sample (m_d) were recorded. The gel content (G (%)) was calculated by the following formulas:

$$G(\%) = \frac{m_d}{m_0} \times 100\% \quad (1)$$

All of these data were measured three times and averaged.

Investigation of the Triple Shape-Memory Effect (TSME). TSME was tested by the bending test.[24,60,61] The film for the test was put into a straight specimen with a dimension of 30 × 6 × 0.5 mm, and the testing was carried out as follows: first, a straight sample (shape A) was bent at a given angle θ_{i1} (θ_{i1} =90°) at T_{high} ($T_{high} > T_{m,\,PCL} > T_{m,\,PTMEG}$) and was kept in this temporary shape B. Then, the deformed shape was quenched to T_{mid} ($T_{m,\,PCL} > T_{mid} > T_{m,\,PTMEG}$) for 10 min, and a fixing angle θ_{f1} was obtained after the bending stress was released. Second, the bending sample was bent again at a given angle θ_{i2} (θ_{i2} = 135°) at T_{mid} and kept for 10 min and then quenched to T_{low} ($T_{m,\,PCL} > T_{m,\,PTMEG} > T_{low}$) for another 10 min, getting temporary shape C. Finally, recovery angles θ_{r1} and θ_{r2} were recorded after the film was reheated to T_{mid} and T_{high}, respectively. The formulas of R_f and R_r are given by

DOI: 10.1021/am507575z
ACS Appl. Mater. Interfaces 2015, 7, 2585−2596

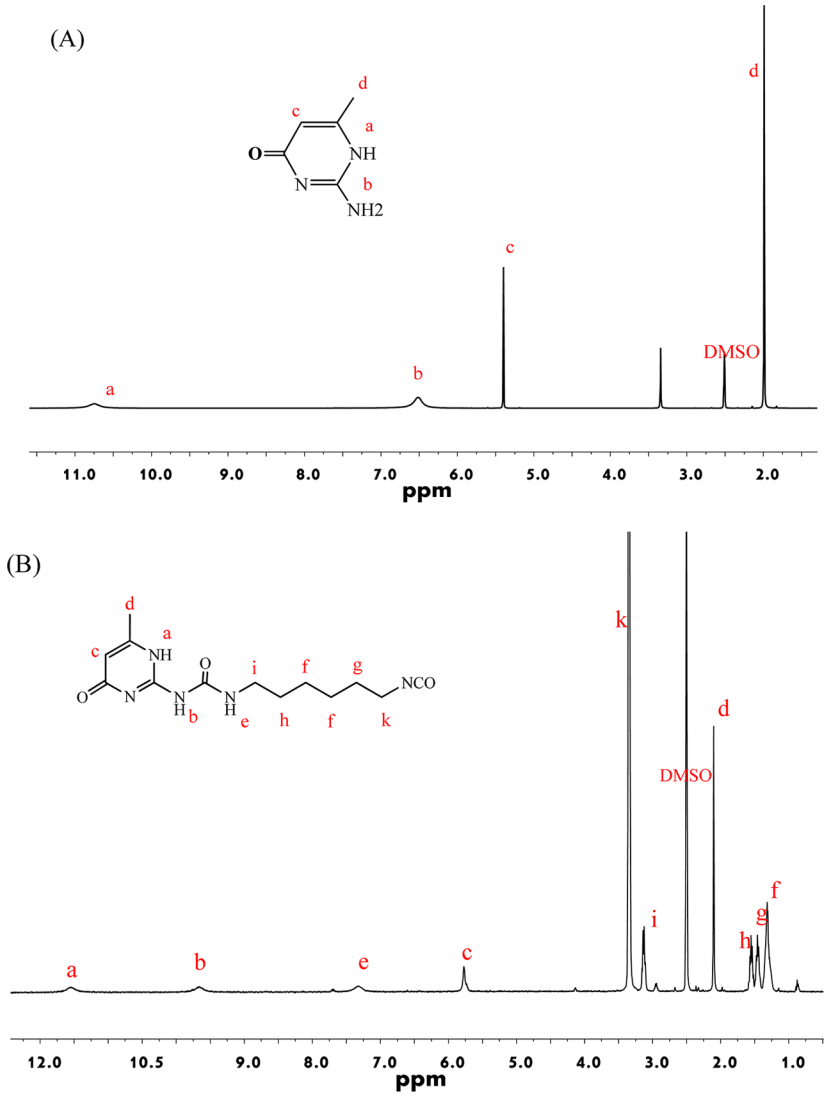

Figure 1. ^{1}H NMR spectra of MIC (A) and UPy (B) in DMSO-d_6.

$$R_{f,A\to B} = \frac{\theta_{f1}}{\theta_{i1}} \times 100\% \quad (2)$$

$$R_{f,B\to C} = \frac{\theta_{f2} - \theta_{f1}}{\theta_{i2} - \theta_{f1}} \times 100\% \quad (3)$$

$$R_{r,C\to B} = \frac{\theta_{f2} - \theta_{r1}}{\theta_{f2} - \theta_{f1}} \times 100\% \quad (4)$$

$$R_{r,C\to A} = \frac{\theta_{f2} - \theta_{r2}}{\theta_{f2}} \times 100\% \quad (5)$$

Investigation of the Self-Healing Effect (SHE). SHE was tested by Instron Universal Testing Machine (Model 4302, Instron Engineering Corporation, Canton, MA). In this work, two strips of a knife-cut and an undamaged strip with an average thickness of 0.30 mm and a width of 4.75 mm cut from each sample were prepared. Then, one of the damaged strips was put into a convection oven for 48 h at 40 °C. After that, all the strips were tested by Instron Universal Testing Machine under a 200 N load cell and uniaxially stretched to a displacement at 50 mm min^{-1}, with a strain rate of 330%/min.

The recovery in performance relative to the pristine material is defined as the healing efficiency. The healing efficiencies (η) have been assessed by the equation below. Here, σ_0 refers to the tensile strength of the pristine strip; meanwhile, σ_h is the tensile strength of the healed sample.

$$\eta\,(\%) = \frac{\sigma_h}{\sigma_o} \times 100\% \quad (6)$$

RESULTS AND DISCUSSION

Characterization of 1-(6-Isocyanate)-3-(6-methyl-4-oxo-1,4-dihydropyrimidin-2-yl) Urea (UPy). UPy was synthesized by the reaction of MIC and HDI (Scheme 1A). Here, MIC was first prepared by reacting guanidine carbonate with EAA in dry ethanol as solvent. The structure of MIC was confirmed by ^{1}H NMR spectroscopy (400 MHz, DMSO-d_6, δ): 10.76 (δH^a, 1 H, s, −NH−, amine of pyrimidinone ring), 6.52 (δH^b, 2 H, s, −NH$_2$, end group amine α to pyrimidinone ring), 5.40 (δH^c, 1 H, s, −CH═), 1.99 (δH^d, 3 H, s, −CH$_3$, end group CH$_3$ α to pyrimidinone). ^{1}H NMR spectroscopy of UPy (400 MHz, DMSO-d_6, δ): 11.54 (δH^k, 1 H, s, amine of pyrimidinone ring), 9.75 (δH^a, 1 H, s, end group urea α to pyrimidinone ring), 7.41 (δH^b, 1 H, s, end group urea), 5.75 (δH^c, 1 H, s, end group pyrimidinone), 3.33 (δH^e, 2 H, t, end group CH$_2$ α to ester), 3.16 (δH^i, 2 H, t, end group CH$_2$ α to urea), 2.10 (δH^d, 3 H, s, end group CH$_3$ α to pyrimidinone),

DOI: 10.1021/am507575z
ACS Appl. Mater. Interfaces 2015, 7, 2585−2596

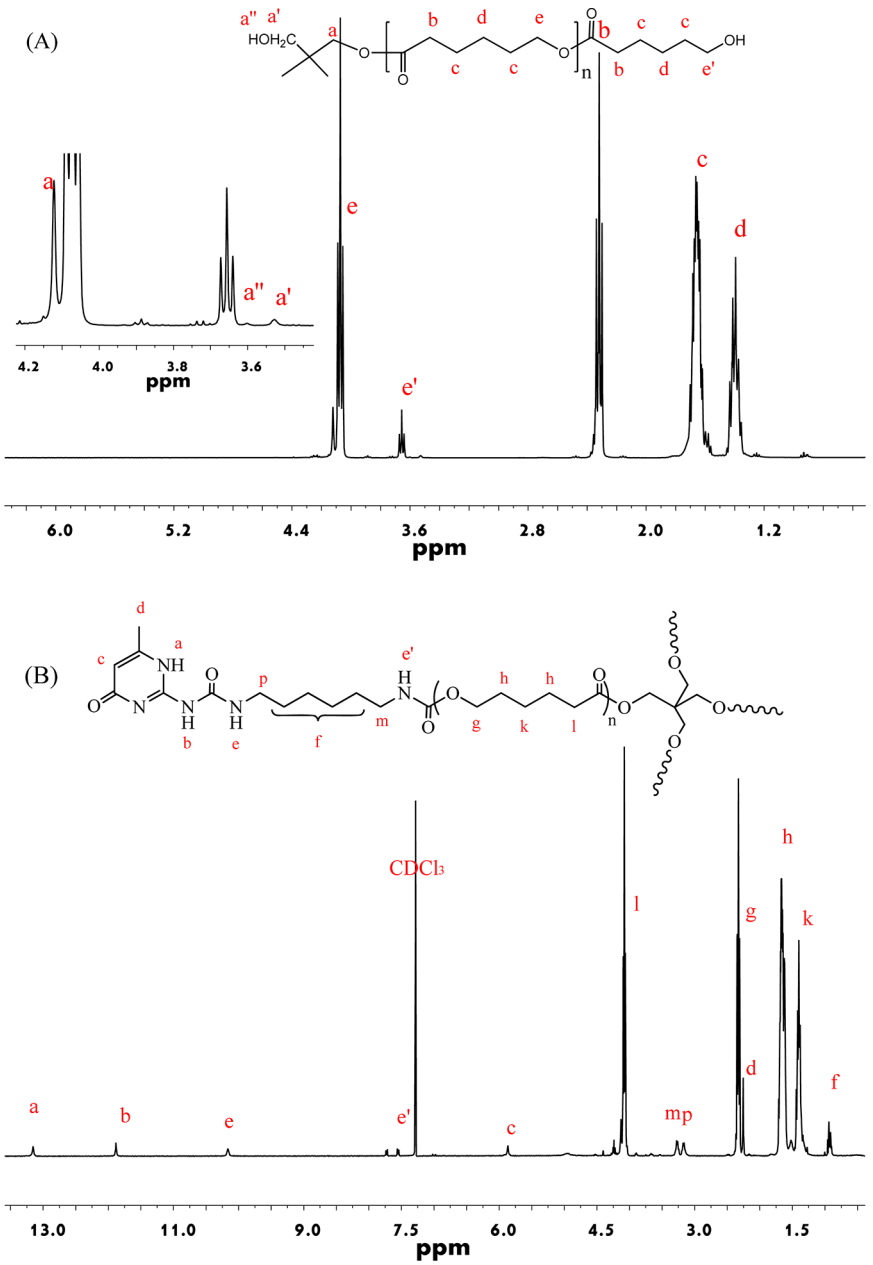

Figure 2. ^{1}H NMR spectra of (A) ^{4}PCL and (B) ^{4}PCL-U in $CDCl_3$.

1.74−0.97 ($\delta H^{h,g,f}$, 8 H, m, the four connected methylenes of HDI). The ^{1}H NMR spectroscopy MIC (A) and UPy (B) are shown in Figure 1.

Characterization of Upy-Functionalized Four-Arm Star-Shaped PCL (^{4}PCL-U). The synthetic route is shown in Scheme 1B. First, ^{4}PCL precursor was synthesized by typical ring-opening polymerization of ε-caprolactone using PTOL as an initiator and $SnOct_2$ as a catalyst. Then, the ^{4}PCL-U was obtained by decorating ^{4}PCL with the UPy end group.[38,40] The structures of ^{4}PCL and ^{4}PCL-U were confirmed by ^{1}H NMR (Figure 2): the characteristic peak of methylene in ^{4}PCL appears at 4.07 ppm (δH^{e}), 2.34 ppm (δH^{b}), 1.68 ppm (δH^{c}), and 1.40 ppm (δH^{d}). The peak at 4.12 ppm (δH^{a}) is the characteristic peak of $-CH_2$ in pentaerythritol which is connected to PCL. The peaks at 3.60 ppm ($\delta H^{a''}$) and 3.53 ppm ($\delta H^{a'}$) are caused by $-CH_2CH_2OH$ in PTOL. Furthermore, the methylene proton of $-CH_2OH$ groups terminating ^{4}PCL appears at 3.65 ppm ($\delta H^{e'}$). The results suggested that the target prepolymer has been successfully synthesized. The M_n of ^{4}PCL prepolymer calculated from ^{1}H NMR is 4300 g mol^{-1}, while this parameter obtained from the GPC test is about 6000 g mol^{-1} with PDI of 1.30. ^{4}PCL-U was also characterized by ^{1}H NMR in $CDCl_3$. Compared with ^{4}PCL, several new signals appear: the peaks at δ = 13.15, 11.89, 10.15, and 5.86 ppm may be assigned to the typical peaks of the UPy group, and the new peak at δ = 7.54 ppm refers to −CO−NH. Meanwhile, the peak at 3.65 ppm disappears. All these features indicate that ^{4}PCL-U has been synthesized successfully.

Characterization of UPy-Functionalized PTMEG (PTMEG-U). PTMEG-U was prepared following the method derived from the literature,[49] which was similar to that of ^{4}PCL-U (Scheme 1C), and the structure of PTMEG-U is confirmed by the ^{1}H NMR spectrum (Figure 3). The characteristic peaks attributed to the UPy group appear at 11.55 ppm (δH^{a}), 9.66

DOI: 10.1021/am507575z
ACS Appl. Mater. Interfaces 2015, 7, 2585−2596

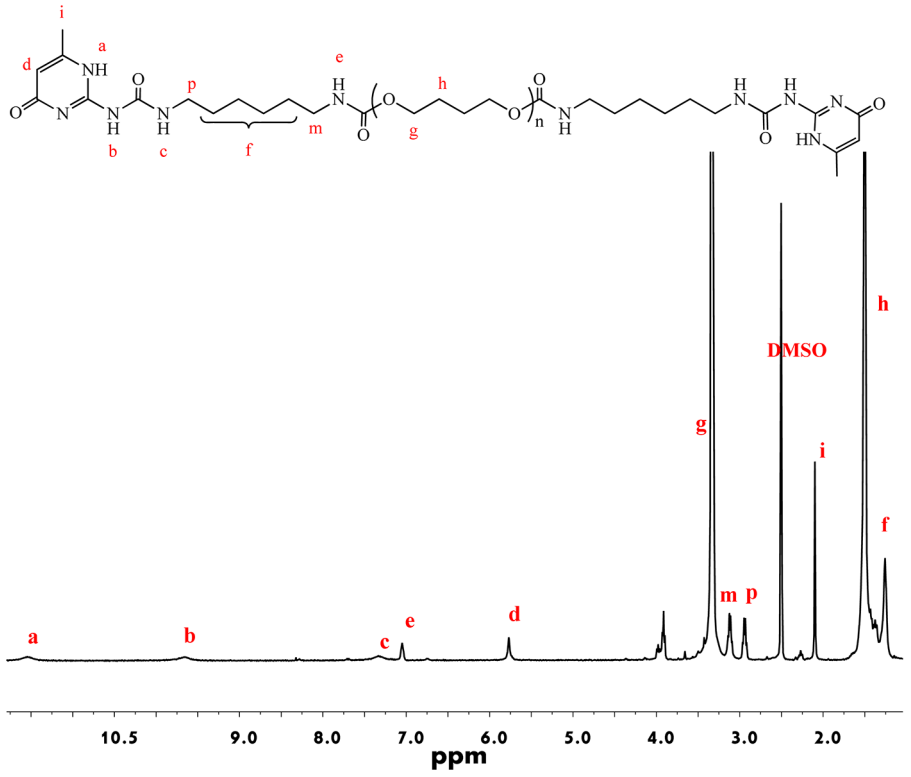

Figure 3. ^{1}H NMR spectrum of PTMEG-U in DMSO-d_6.

Scheme 2. Schematic Route of the PCL−PTMEG Network

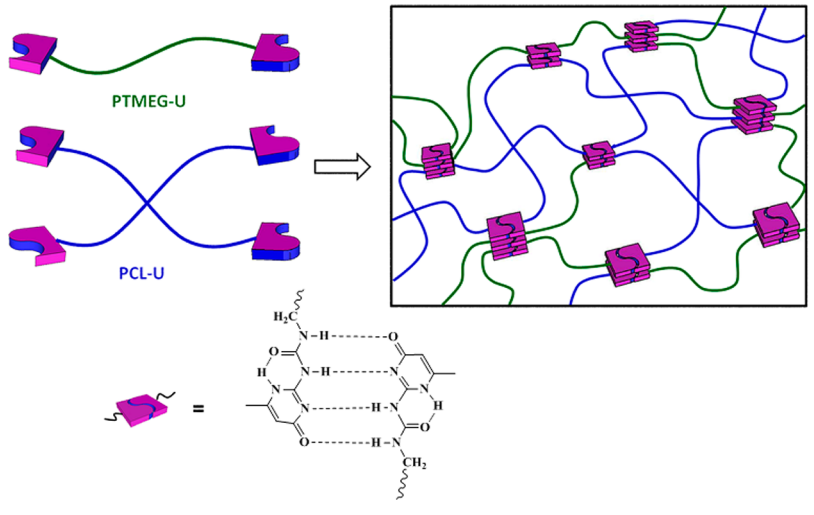

ppm (δH^{b}), 7.32 ppm (δH^{c}), and 5.76 ppm (δH^{d}), while the characteristic peaks of methylene in the PTMEG repeat units appear at 3.33 ppm (δH^{g}) and 1.50 ppm (δH^{h}). Moreover, the new peak at 7.04 ppm (δH^{e}) belongs to the proton of the amine next to $-COOCH_2$, and the area of the peak is equivalent with the peak δH^{a}.

Characterization of PCL−PTMEG Networks. The PCL−PTMEG networks were prepared by the dimerization of UPy between [4]PCL-U and PTMEG-U in chloroform (Scheme 2). A series of networks with different compositions were prepared; the feed ratio and the swelling test results were list in Table 1.

Meijer and co-workers have reported that, in a polar aprotic solvent, such as DMSO, the Upy existed in the 6[1*H*]-pyrimidinone monomeric form, which could not form dimers,

Table 1. Feed Ratio and Gel Content of PCL−PTMEG Networks

sample	PCL−PTMEG (wt/wt)	*G* (%)
PCL_{20}−$PTMEG_{80}$	20:80	82 ± 1.0
PCL_{36}−$PTMEG_{64}$	36:64	83 ± 1.4
PCL_{50}−$PTMEG_{50}$	50:50	95 ± 1.1
PCL_{64}−$PTMEG_{36}$	64:36	93 ± 2.2
PCL_{80}−$PTMEG_{20}$	80:20	90 ± 3.4

whereas in less polar solvents, such as $CDCl_3$, Upy existed as a mixture of the 4[1*H*]-pyrimidinone and pyrimidin-4-ol which could dimerize via DDAA and DADA array, respectively, and high dimerization constants were all observed.[46−48] In this work, we just utilize this nature of the Upy group which can

DOI: 10.1021/am507575z
ACS Appl. Mater. Interfaces 2015, 7, 2585−2596

associate and disassociate in different solvents to construct the reversible network. To identify this feature, ^{1}H NMR and FT-IR techniques were employed. Figure 4A illustrates the ^{1}H

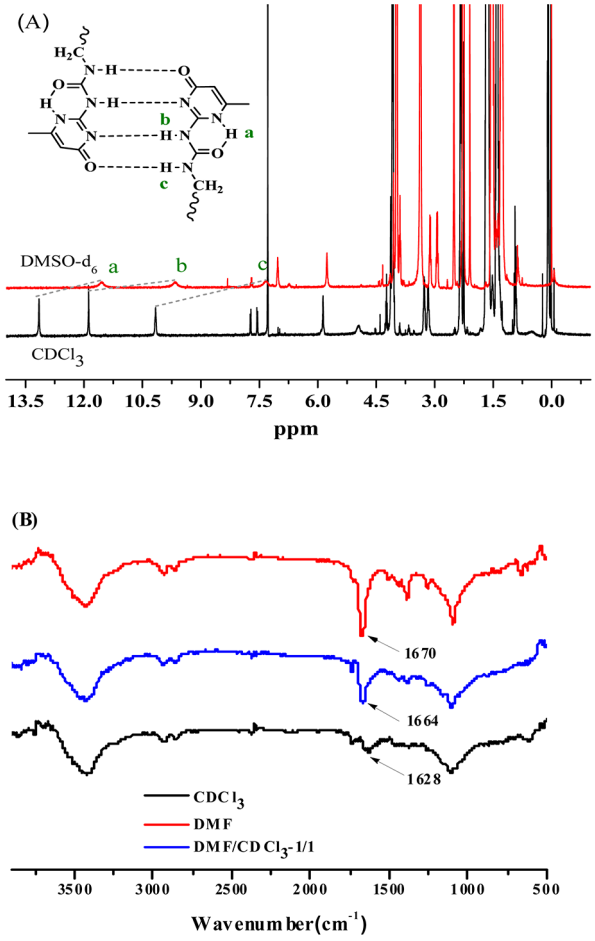

Figure 4. (A) ^{1}H NMR spectra of the ^{4}PCL-U in $CDCl_3$ and DMSO-d_6. (B) FT-IR Spectra of the PCL_{50}–$PTMEG_{50}$ network in solvents with different polarity.

NMR spectra of the ^{4}PCL-U and the protons H^a, H^b, and H^c which in $CDCl_3$ shifted downfield compared with that in DMSO-d_6, indicating these protons were involved in intermolecular hydrogen bonds. Figure 4B shows the FT-IR spectra of the PCL_{50}-$PTMEG_{50}$ network in solvents with different polarity. Obviously, the stretching vibration of carbonyl on the pyrimidinone ring of UPy shifts to lower wavenumber while increasing the equiv of $CHCl_3$/DMF. This phenomenon may be ascribed to the formation of quadruple hydrogen bonds between the UPy end group resulting in the stretching vibration of the carbonyl bathochromic shift and the reduction of free carbonyls lessening the amplitude.

Thermal Behavior of PTMEG–PCL Networks. Particularly, the thermal behavior is very important for the thermally induced SMPs. It not only determines the transition temperature but also dominates the shape memory performance. In this work, the crystallization behavior of the PCL–PTMEG networks with different component ratios were investigated by DSC. Figure 5 displays the thermograms of all the samples in a cooling scan (A) and the following heating scan (B), and the relevant thermal parameters and their corresponding values are summarized in Table 2.

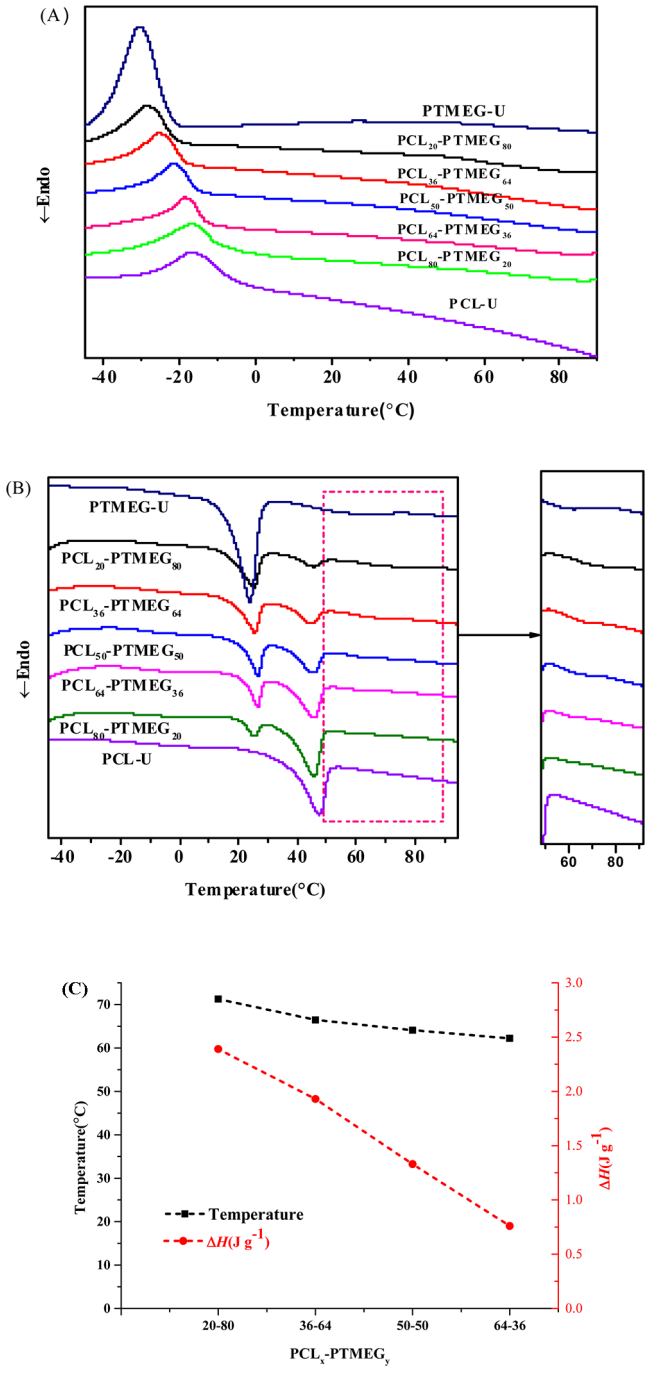

Figure 5. DSC curves of the PCL–PTMEG networks. (A) Cooling run after melt quenching at a rate of 5 °C min^{-1}. (B) Subsequent heating run at a rate of 5 °C min^{-1}. (C) Temperature and ΔH_m^c vs PCL_x–$PTMEG_y$ for all samples.

In Figure 5, the two precursors PTMEG-U and ^{4}PCL-U show obvious crystalline exothermic peaks at −31.32 and −15.19 °C in the cooling run (A), respectively, corresponding with melting endothermic peaks at 24.6 and 46.6 °C in following heating run (B), respectively. For PTMEG–PCL networks, however, only one broad crystalline exothermic peak is observed in the cooling run although two individual separate melting endothermic peaks are detected in following heating run. We speculate it may be caused by the overlap of two crystalline peaks for PTMEG and PCL segments since the two crystalline temperatures are quite close, and it can be proven by

DOI: 10.1021/am507575z
ACS Appl. Mater. Interfaces 2015, 7, 2585–2596

Table 2. DSC Data of the PCL−PTMEG Networks

	first cooling scan		subsequent heating scan					
sample	T_c (°C)	ΔH_c (J g^{-1})	T_m^a (°C)	ΔH_m^a (J g^{-1})	T_m^b (°C)	ΔH_m^b (J g^{-1})	T_m^c (°C)	ΔH_m^c (J g^{-1})
PTMEG-U	−31.3	28.4	24.6	29.8			60.5	4.0
PCL_{20}−$PTMEG_{80}$	−25.5	22.4	23.4	19. 9	43.6	4.7	76.7	2.7
PCL_{36}−$PTMEG_{64}$	−19.1	22.7	24.5	15.0	44.2	9.1	64.8	1.3
PCL_{50}−$PTMEG_{50}$	−17.4	20.4	25.6	11.2	45.0	11.1	63.8	1.2
PCL_{64}−$PTMEG_{36}$	−15.2	26.0	25.2	11.1	45.5	21.2	61.5	0.8
PCL_{80}−$PTMEG_{20}$	−13.8	25.3	25.1	6.2	45.8	25.9		
^{4}PCL-U	−15.2	26.0			46.6	35.2		

the fact that the crystalline enthalpy (ΔH_c) is a match with the sum of two melting enthalpies (ΔH_m). As we know, PTMEG and PCL segments will be restrained reciprocally after being incorporated into one network. Thus, it is easy to understand that the crystallization behavior is affected by the composition of networks. It makes sense that the crystallization degree of the PTMEG segments increases with its content, and the crystalline temperature (T_c) of the network is close to that of PTMEG-U. It also works for PCL segments. When the content of PTMEG segments increased from 20% to 80%, melting enthalpy of PTMEG segments (ΔH_m^b) increased from 6.2 to 19.9 J g^{-1}; contrarily, the melting enthalpy of the PCL segment (ΔH_m^c) decreased from 25.7 to 4.9 J g^{-1}. Meanwhile, the T_c shifted from −13.8 to −25.5 °C, getting close to the T_c of PTMEG gradually, even though there is no distinct change for ΔH_c. Although the crystallization degree of each segment varied with the composition, the melting temperatures of the two segments (T_m^b and T_m^c) have no obvious change, and the difference is about 20 °C, ensuring that the T_{trans} values act like those in a triple-shape memory system.

Besides two distinct melting endothermic peaks in the heating run, another weak endothermic peak was also observed in a range from 61.54 to 71.71 °C. Sijbesma and co-workers have reported that lateral aggregation of the UPy groups can be observed when there is a urethane or urea group next to the UPy groups in an Upy-telechelic supramolecular system.[62] The lateral aggregation was ascribed to the directionality of the hydrogen bonds between the urethane groups or urea groups. In present work, there also was a urethane group next to the UPy group. We speculate that this endothermic signal is the melting peak of aggregated UPy (T_m^c). Moreover, the melting enthalpies (ΔH_m^c) range from 0.83 to 2.72 J g^{-1}, while the content of PTMEG increased from 36% to 80% (Figure 5C). As we know, PTMEG-U is a linear precursor and ^{4}PCL-U is a four-armed PCL precursor. Increasing the content of PTMEG segments will reduce the cross-linking density of the network, and it will benefit the aggregation of the UPy group.

Dynamic Mechanical Analysis of the PTMEG−PCL Networks. The dynamic mechanical properties of PCL−PTMEG networks were characterized by DMA, and the corresponding results are presented in Figure 6. It shows the storage modulus (E') as a function of temperature for the PCL−PTMEG networks, and the results are presented in Table 3. A large difference in modulus below and above the T_{trans} (e.g., $T_{m,\,PTMEG}$ and $T_{m,\,PCL}$) is the most substantial property to render shape memory function. Polymers with a larger storage modulus ratio (E'_{below}/E'_{above}) have a better shape memory effect for easier high temperature deformation and maintaining the deformation at low temperature.[63] As a triple-shape memory polymer in this work, three typical moduli $E'_{10\,°C}$, $E'_{40\,°C}$, and $E'_{70\,°C}$ are noted, which correspond to the storage modulus at

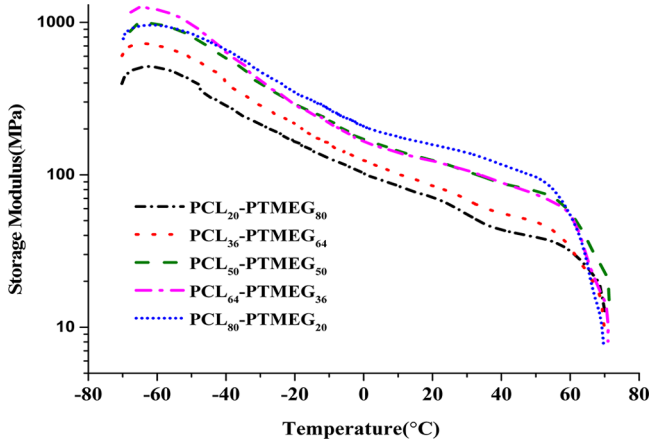

Figure 6. Storage modulus−temperature curves of PCL−PTMEG networks.

T_{low}, T_{mid}, and T_{high}, respectively. Here, it is clearly seen that all samples display two plateaus corresponding to the melting of PTMEG and PCL segments, and a pronounced decrease in E' is observed below and above both the two T_{trans} values. According to the result of DSC analysis, increasing the PTMEG segment will enhance the crystallization of PTMEG, and consequently, the polymers show a higher $E'_{10\,°C}/E'_{40\,°C}$ value; on the contrary, increasing the PCL segment will enhance the crystallization of PCL, and consequently, the polymers showed a higher $E'_{40\,°C}/E'_{70\,°C}$ value. On the basis of this result, we can predict that the PCL−PTMEG networks possess an ideal thermal mechanical feature to program the triple-shape effect.

Triple Shape-Memory Effect. In the present work, the bending test was employed to investigate the shape memory effect of the PCL−PTMEG networks, and the determined fixity ratio (R_f) and the recovery ratio (R_r) are tabulated in Table 4. From the view of the molecular design, the crystalline PCL and PTMEG segments act as two switch domains, and the networks constructed by dimerization of Upy groups play a role of netpoints of this SMP. Actually, the composition of the network affects the R_f and R_r to a certain extent. It is easy to understand that the shape fixity lies on the physical cross-linking formed by the crystallization of soft segment. From the analysis of DSC, we knew that all samples were double crystalline, which ensures that all could display a triple-shape memory effect. In reality, $R_{f,\,A\to B}$ and $R_{f,\,B\to C}$ values remain quite high and vary slightly with the composition; for example, the $R_{f,\,A\to B}$ increased from 95.6% to 98.9% as the weight content of PCL increased from 20% to 80%. In the recovery program, $R_{r,\,C\to B}$ has better performance than $R_{r,\,C\to A}$ except the sample with the lowest PTMEG content. It can be explained that both the physical cross-linking formed by the crystalline

DOI: 10.1021/am507575z
ACS Appl. Mater. Interfaces 2015, 7, 2585−2596

Table 3. Relevant Data for the PCL−PTMEG Networks Resulting from the DMA Analysis

sample	storage modulus (MPa)			$r_{E'1}$ ($E'_{10\ °C}/E'_{40\ °C}$)	$r_{E'2}$ ($E'_{40\ °C}/E'_{70\ °C}$)
	10 °C	40 °C	70 °C		
PCL_{20}−$PTMEG_{80}$	84.40	43.52	13.31	1.94	3.27
PCL_{36}−$PTMEG_{64}$	101.50	55.99	15.40	1.81	3.63
PCL_{50}−$PTMEG_{50}$	143.50	88.34	23.20	1.62	3.81
PCL_{64}−$PTMEG_{36}$	139.30	88.96	14.83	1.56	6.00
PCL_{80}−$PTMEG_{20}$	177.70	116.90	7.61	1.52	15.36

Table 4. Triple-Shape Memory Performance of the PCL−PTMEG Networks

sample	$R_{f,\ A\to B}$ (%)	$R_{f,\ B\to C}$ (%)	$R_{r,\ C\to B}$ (%)	$R_{r,\ C\to A}$ (%)
PCL_{20}−$PTMEG_{80}$	95.6 ± 0.5	90.7 ± 2.1	83.9 ± 5.0	62.3 ± 0.5
PCL_{36}−$PTMEG_{64}$	97.8 ± 0.5	90.5 ± 0.1	94.8 ± 2.7	71.0 ± 1.2
PCL_{50}−$PTMEG_{50}$	98.3 ± 1.1	87.9 ± 2.3	97.2 ± 2.8	73.2 ± 1.4
PCL_{64}−$PTMEG_{36}$	97.2 ± 1.2	91.8 ± 1.1	110.5 ± 7.5	73.9 ± 0.7
PCL_{80}−$PTMEG_{20}$	98.9 ± 1.2	90.4 ± 2.9	44.6 ± 1.7	75.0 ± 1.4

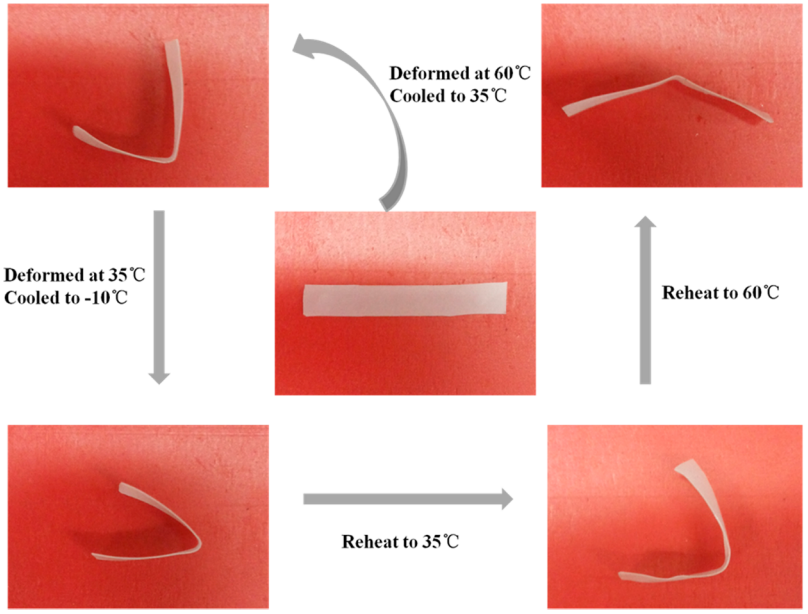

Figure 7. Triple-shape memory effect of a strip sample of PCL_{36}−$PTMEG_{64}$.

PCL segment and the chemical cross-linking formed by the dimerization of the Upy group can serve as netpoints during the recovery process from shape C to shape B; otherwise, only the latter can act as netpoints during the recovery process from shape B to shape A. As we know, the [4]PCL-U precursor is a four-armed star-shape prepolymer while PTMEG-U is a linear prepolymer; thus, increasing the content of the PCL segment should increase the density of netpoints, and the $R_{r,\ C\to A}$ should increase in theory accordingly. In fact, $R_{r,\ C\to A}$ was enhanced indistinctively from 71% to 75% with the content of PCL increasing from 36% to 80%. It may be ascribed to the stronger aggregation of Upy dimers in the sample with a higher PTMEG segment, which may make up the decrease of the netpoints density.

The triple-shape memory effect of the PCL−PTMEG network was also recorded by a digital photo in programming (Figure 7). The shape memory effect proceeds as follows: in the beginning, the sample with permanent shape A was heated to T_{high} = 60 °C, above the T_m of both the PTMEG and PCL segments. Then, the deformed sample was cooled to T_{mid} = 35 °C; the crystal of the PCL segment was established with the external stress kept on. As soon as the stress was released, temporary shape B was achieved. Afterward, the shape B was deformed under stress and cooled to T_2 = −10 °C; then, the external stress was removed, and after cooling, the result was temporary shape C. For recovery, the sample was heated to T_{mid} = 35 °C, obtaining shape B, and it was stable until elevating the temperature to T_1 = 60 °C, which led the sample to recover the permanent shape A. Qualitatively, under these thermal conditions, the sample displayed a passable triple-shape memory effect.

Self-Healing Behavior. Indeed, the PTMEG−PCL network constructed by self-complementary quadruple hydrogen bonding has a dynamic feature. We predict it should exhibit intrinsic self-healing ability. Then, the damaging and self-healing tests were conducted. After damaging a sample with a razor blade and gently warming it in a convection oven at 40 °C for 48 h, the self-healing effect was achieved without any external healing agents or solvent.

The tensile test was carried out to evaluate the efficiency of self-healing. The tensile strength (σ) and elongation at break (ε) of each sample before damage, after damage, and after

DOI: 10.1021/am507575z
ACS Appl. Mater. Interfaces 2015, 7, 2585−2596

Table 5. Tensile Strength (σ), Elongation at Break (ε), and Healing Efficiencies (η) of All Samples during Healing Test

	σ (MPa)			ε (%)			
sample	original	damaged	healed	original	damaged	healed	η (%)
PCL_{20}–$PTMEG_{80}$	3.24 ± 0.20	2.63 ± 0.16	2.81 ± 0.03	54.38 ± 3.80	24.04 ± 2.27	32.74 ± 1.47	87.93
PCL_{36}–$PTMEG_{64}$	3.78 ± 0.10	2.03 ± 0.11	2.83 ± 0.37	44.90 ± 5.45	19.14 ± 3.57	28.08 ± 3.01	76.25
PCL_{50}–$PTMEG_{50}$	4.92 ± 0.07	2.62 ± 0.19	3.23 ± 0.78	43.94 ± 7.46	20.45 ± 0.72	31.35 ± 0.78	69.56
PCL_{64}–$PTMEG_{36}$	6.03 ± 0.10	2.75 ± 0.23	3.94 ± 0.04	26.66 ± 0.21	13.41 ± 3.75	21.72 ± 0.21	65.34
PCL_{80}–$PTMEG_{20}$	8.25 ± 0.27	5.06 ± 0.12	5.62 ± 0.22	18.13 ± 2.71	21.69 ± 0.67	19.39 ± 1.75	63.01

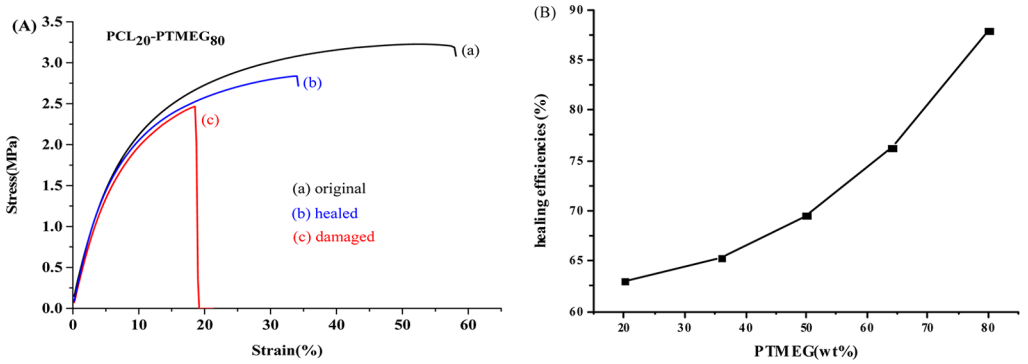

Figure 8. Self-healing tests for the PCL–PTMEG networks. (A) Typical engineering stress–strain curve for PCL_{20}–$PTMEG_{80}$ networks; (B) the variation tendency of healing efficiencies against the mass fraction of the PTMEG segment.

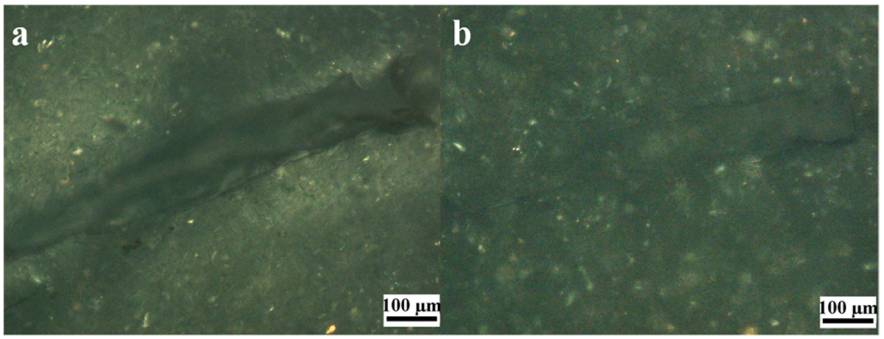

Figure 9. Optical micrographs of the PCL–PTMEG specimen: (a) before healing treatment; (b) heated to 40 °C and kept for 2 h.

healing are summarized in Table 5, and the efficiency of self-healing is calculated by eq 6. Here, only a typical engineering stress–strain curve of PCL_{20}–$PTMEG_{80}$ is shown in Figure 8A. For the pristine strips, σ increases with an increase in the content of the PCL segment, while ε has the opposite variation tendency. It makes sense that the tensile property of the sample is more close to the polymer in the dominant portion. After being damaged, the notched specimen failed immediately at the fracture and showed very poor tensile property. After healing, however, both σ and ε were enhanced obviously compared to the notched specimen. In addition, the self-healing efficiencies of the PCL–PTMEG networks increased with the increase of the PTMEG segment content and achieved optimal healing of up to 87% recovery of σ relative to a pristine sample when the PTMEG content was 80% (Figure 8B). As we know, the self-healing capacity of this dynamic network is derived from the dissociation of the quadruple hydrogen bonding during the damage and reassociation during the healing process. Hence, the mobility of the soft segment will affect the possibility of the terminal Upy groups to meet each other and dimerize. From the DSC analysis above, we know that the T_m of the PTMEG segment ranges from 23.4 to 25.6 °C by varying the composition, so it stays in the molten state at the healing temperature of 40 °C. Therefore, it is easier for the PTMEG segment chains to move and be in contact with each other in the damaged area, which helps the dangling hydrogen bonds exposed on the freshly crack surface to find new interaction partners to rebuild the self-complementary hydrogen bonding.

The self-healing effect of the PTMEG–PCL dynamic network was also recorded by an optical microscope (Figure 9). First, the sample was scraped with a fresh razor blade and a crack was observed (Figure 9a); then, the sample was heated to 40 °C and kept for 2 h. The crack was almost healed (Figure 9b).

CONCLUSION

In conclusion, a series of PCL–PTMEG dynamic networks with different composition was synthesized successfully via self-complementary quadruple hydrogen bonding through Upy-telechelic PTMEG and [4]PCL precursors. During the heating scan of DSC analysis, dynamic networks possess three discrete thermal transitions which belong to the melting of the PTMEG and PCL segment and the aggregation of Upy dimers, respectively. The PTMEG and PCL segment act as the switching domains, and the dimerization of the UPy units accompanied by its aggregation serve as netpoints in a TSP

DOI: 10.1021/am507575z
ACS Appl. Mater. Interfaces 2015, 7, 2585–2596

system. In the TSE test, the fixing ratios (R_f) of networks range from 84% to 99%, which quite correspond to the crystallization of the switching segments. In a broad composition range, there is no evident change in the whole recovery ratios ($R_{r\ C\to A}$), since the netpoints consisted of the dimerization of Upy and its aggregation. The self-healing effect of the samples was also evaluated. The highest healing efficiency is 88%, corresponding to the sample containing an 80 wt % PTMEG segment.

AUTHOR INFORMATION

Corresponding Author

*E-mail: kkyangscu@126.com. Fax: 86-28-85410755. Tel: 86-28-85410755.

Notes

The authors declare no competing financial interest.

ACKNOWLEDGMENTS

This work was supported financially by the National Science Foundation of China (51273120, 51473096) and the Program for Changjiang Scholars and Innovative Research Team in University of Ministry of Education of China (IRT1026).

REFERENCES

(1) Huang, W. M.; Ding, Z.; Wang, C. C.; Wei, J.; Zhao, Y.; Purnawali, H. Shape Memory Materials. *Mater. Today* **2010**, *13*, 54−61.

(2) Sun, L.; Huang, W. M.; Wang, C. C.; Zhao, Y.; Ding, Z.; Purnawali, H. Optimization of The Shape Memory Effect in Shape Memory Polymers. *J. Polym. Sci., Part A: Polym. Chem.* **2011**, *49*, 3574−3581.

(3) Huang, W. M.; Yang, B.; Zhao, Y.; Ding, Z. Thermo-Moisture Responsive Polyurethane Shape-Memory Polymer and Composites: A Review. *J. Mater. Chem.* **2010**, *20*, 3367−3381.

(4) Kumpfer, J. R.; Rowan, S. J. Thermo-, Photo-, and Chemo-Responsive Shape-Memory Properties from Photo-Cross-Linked Metallo-Supramolecular Polymers. *J. Am. Chem. Soc.* **2011**, *133*, 12866−12874.

(5) Ratna, D.; Karger-Kocsis, J. Recent Advances in Shape Memory Polymers and Composites: A Review. *J. Mater. Sci.* **2008**, *43*, 254−269.

(6) Lendlein, A.; Jiang, H.; Junger, O.; Langer, R. Light-Induced Shape-Memory Polymers. *Nature* **2005**, *434*, 879−882.

(7) Garle, A.; Kong, S.; Ojha, U.; Budhlall, B. M. Thermoresponsive Semicrystalline Poly(ε-caprolactone) Networks: Exploiting Cross-Linking with Cinnamoyl Moieties to Design Polymers with Tunable Shape Memory. *ACS Appl. Mater. Interfaces* **2012**, *4*, 645−657.

(8) Sun, L.; Huang, W. M. Mechanisms of the Multi-Shape Memory Effect and Temperature Memory Effect in Shape Memory Polymers. *Soft Matter* **2010**, *6*, 4403−4406.

(9) Metzger, M.; Wilson, T.; Schumann, D.; Matthews, D.; Maitland, D. Mechanical Properties of Mechanical Actuator for Treating Ischemic Stroke. *Biomed. Microdevices* **2002**, *4* (2), 89−96.

(10) Small, W., IV; Wilson, T.; Benett, W.; Loge, J.; Maitland, D. Laser-Activated Shape Memory Polymer Intravascular Thrombectomy Device. *Opt. Express* **2005**, *13* (20), 8204−8213.

(11) Yu, X.; Zhou, S.; Zheng, X.; Xiao, Y.; Guo, T. Influence of in Vitro Degradation of a Biodegradable Nanocomposite on Its Shape Memory Effect. *J. Phys. Chem. C* **2009**, *113*, 17630−17635.

(12) Metcalfe, A.; Desfaits, A.-C.; Salazkin, I.; Yahia, L. H.; Sokolowski, W. M.; Raymond, J. Cold Hibernated Elastic Memory Foams for Endovascular Interventions. *Biomaterials* **2003**, *24*, 491−497.

(13) Lendlein, A.; Kelch, S. Shape-Memory Polymers as Stimuli-Sensitive Implant Materials. *Clin. Hemorheol. Microcirc.* **2005**, *32*, 105−116.

(14) Huang, W. M.; Song, C. L.; Fu, Y. Q.; Wang, C. C.; Zhao, Y.; Purnawali, H.; Lu, H. B.; Tang, C.; Ding, Z.; Zhang, J. L. Shaping Tissue with Shape Memory Materials. *Adv. Drug Delivery Rev.* **2013**, *65*, 515−535.

(15) Wang, S. Q.; Kaneko, D.; Okajima, M.; Yasaki, K.; Tateyama, S.; Kaneko, T. Hyperbranched Polycoumarates with Photofunctional Multiple Shape Memory. *Angew. Chem., Int. Ed.* **2013**, *52*, 11143−11148.

(16) Pilate, F.; Mincheva, R.; De Winter, J.; Gerbaux, P.; Wu, L.; Todd, R.; Raquez, J. M.; Dubois, P. Design of Multistimuli-Responsive Shape-Memory Polymer Materials by Reactive Extrusion. *Chem. Mater.* **2014**, *26*, 5860−5867.

(17) Nair, K. P.; Breedveld, V.; Weck, M. Multiresponsive Reversible Polymer Networks Based on Hydrogen Bonding and Metal Coordination. *Macromolecules* **2011**, *44*, 3346−3357.

(18) Wang, L.; Yang, X.; Chen, H.; Yang, G.; Gong, T.; Li, W.; Zhou, S. Multi-Stimuli Sensitive Shape Memory Poly(vinyl alcohol)-Graft-Polyurethane. *Polym. Chem.* **2013**, *4*, 4461−4468.

(19) Behl, M.; Razzaq, M. Y.; Lendlein, A. Multifunctional Shape-Memory Polymers. *Adv. Mater.* **2010**, *22*, 3388−3410.

(20) Huang, W. M.; Zhao, Y.; Wang, C. C.; Ding, Z.; Purnawali, H.; Tang, C.; Zhang, J. L. Thermo/Chemo-Responsive Shape Memory Effect in Polymers: A Sketch of Working Mechanisms, Fundamentals and Optimization. *J. Polym. Res.* **2012**, *19*, 1−34.

(21) Sun, L.; Huang, W. M.; Lu, H.; Lim, K. J.; Zhou, Y.; Wang, T. X.; Gao, X. Y. Heating-Responsive Shape-Memory Effect in Thermoplastic Polyurethanes with Low Melt-Flow Index. *Macromol. Chem. Phys.* **2014**, *215*, 2430−2436.

(22) Liu, C.; Qin, H.; Mather, P. T. Review of Progress in Shape-Memory Polymers. *J. Mater. Chem.* **2007**, *17*, 1543−1558.

(23) Hu, J.; Zhu, Y.; Huang, H.; Lu, J. Recent Advances in Shape-Memory Polymers: Structure, Mechanism, Functionality, Modeling and Applications. *Prog. Polym. Sci.* **2012**, *37*, 1720−1763.

(24) Lendlein, A.; Kelch, S. Shape-Memory Polymers. *Angew. Chem., Int. Ed.* **2002**, *41*, 2034−2057.

(25) Bellin, I.; Kelch, S.; Lendlein, A. Dual-Shape Properties of Triple-Shape Polymer Networks with Crystallizable Network Segments and Grafted Side Chains. *J. Mater. Chem.* **2007**, *17*, 2885−2891.

(26) Behl, M.; Bellin, I.; Kelch, S.; Wagermaier, W.; Lendlein, A. One-Step Process for Creating Triple-Shape Capability of AB Polymer Networks. *Adv. Funct. Mater.* **2009**, *19*, 102−108.

(27) Xie, T.; Xiao, X.; Cheng, Y.-T. Revealing Triple-Shape Memory Effect by Polymer Bilayers. *Macromol. Rapid Commun.* **2009**, *30*, 1823−1827.

(28) Luo, X.; Mather, P. T. Triple-Shape Polymeric Composites (TSPCs). *Adv. Funct. Mater.* **2010**, *20*, 2649−2656.

(29) Bai, Y.; Jiang, C.; Wang, Q.; Wang, T. Multi-Shape-Memory Property Study of Novel Poly(ε-Caprolactone)/Ethyl Cellulose Polymer Networks. *Macromol. Chem. Phys.* **2013**, *214*, 2465−2472.

(30) Ware, T.; Hearon, K.; Lonnecker, A.; Wooley, K. L.; Maitland, D. J.; Voit, W. Triple-Shape Memory Polymers Based on Self-Complementary Hydrogen Bonding. *Macromolecules* **2012**, *45*, 1062−1069.

(31) Xie, T. Tunable Polymer Multi-Shape Memory Effect. *Nature* **2010**, *464*, 267−270.

(32) Luo, Y.; Guo, Y.; Gao, X.; Li, B.-G.; Xie, T. A General Approach Towards Thermoplastic Multishape-Memory Polymers via Sequence Structure Design. *Adv. Mater.* **2013**, *25*, 743−748.

(33) Li, J.; Liu, T.; Xia, S.; Pan, Y.; Zheng, Z.; Ding, X.; Peng, Y. A Versatile Approach to Achieve Quintuple-Shape Memory Effect by Semi-Interpenetrating Polymer Networks Containing Broadened Glass Transition and Crystalline Segments. *J. Mater. Chem.* **2011**, *21*, 12213−12217.

(34) Behl, M.; Lendlein, A. Triple-Shape Polymers. *J. Mater. Chem.* **2010**, *20*, 3335−3345.

(35) Wang, L.; Yang, X.; Chen, H.; Gong, T.; Li, W.; Yang, G.; Zhou, S. Design of Triple-Shape Memory Polyurethane with Photo-Cross-Linking of Cinnamon Groups. *ACS Appl. Mater. Interfaces* **2013**, *5*, 10520−10528.

(36) Zhang, J.; Niu, Y.; Huang, C.; Xiao, L.; Chen, Z.; Yang, K.; Wang, Y. Self-Healable and Recyclable Triple-Shape PPDO-PTMEG

DOI: 10.1021/am507575z
ACS Appl. Mater. Interfaces 2015, 7, 2585−2596

Co-Network Constructed Through Thermoreversible Diels-Alder Reaction. *Polym. Chem.* **2012**, *3*, 1390−1393.
(37) Niu, Y.; Zhang, P.; Zhang, J.; Xiao, L.; Yang, K.; Wang, Y. Poly(p-dioxanone)-Poly(ethylene glycol) Network: Synthesis, Characterization, and Its Shape Memory Effect. *Polym. Chem.* **2012**, *3*, 2508−2516.
(38) Xiao, L.; Wei, M.; Zhan, M.; Zhang, J.; Xie, H.; Deng, X.; Yang, K.; Wang, Y. Novel Triple-Shape PCU/PPDO Interpenetrating Polymer Networks Constructed by Self-Complementary Quadruple Hydrogen Bonding and Covalent Bonding. *Polym. Chem.* **2014**, *5*, 2231−2241.
(39) Jin, Y.; Yu, C.; Denman, R. J.; Zhang, W. Recent Advances in Dynamic Covalent Chemistry. *Chem. Soc. Rev.* **2013**, *42* (16), 6634−6654.
(40) Raquez, J. M.; Vanderstappen, S.; Meyer, F.; Verge, P.; Alexandre, M.; Thomassin, J. M.; Jérôme, C.; Dubois, P. Design of Cross-Linked Semicrystalline Poly(ε-caprolactone)-Based Networks with One-Way and Two-Way Shape-Memory Properties through Diels−Alder Reactions. *Chem.—Eur. J.* **2011**, *17*, 10135−10143.
(41) Ninh, C.; Bettinger, C. J. Reconfigurable Biodegradable Shape-Memory Elastomers via Diels-Alder Coupling. *Biomacromolecules* **2013**, *14*, 2162−2170.
(42) Brunsveld, L.; Folmer, B. J. B.; Meijer, E. W.; Sijbesma, R. P. Supramolecular Polymers. *Chem. Rev.* **2001**, *101*, 4071−4098.
(43) Wang, R.; Xie, T. Shape Memory- and Hydrogen Bonding-Based Strong Reversible Adhesive System. *Langmuir* **2010**, *26*, 2999−3002.
(44) Nair, K. P.; Breedveld, V.; Weck, M. Complementary Hydrogen-Bonded Thermoreversible Polymer Networks with Tunable Properties. *Macromolecules* **2008**, *41*, 3429−3438.
(45) Lawler, A. Government Bows Out of Academy Case. *Science* **1997**, *278*, 28.
(46) Beijer, F. H.; Kooijman, H.; Spek, A. L.; Sijbesma, R. P.; Meijer, E. W. Self-Complementarity Achieved through Quadruple Hydrogen Bonding. *Angew. Chem., Int. Ed.* **1998**, *37*, 75−78.
(47) Beijer, F. H.; Sijbesma, R. P.; Kooijman, H.; Spek, A. L.; Meijer, E. W. Strong Dimerization of Ureidopyrimidones via Quadruple Hydrogen Bonding. *J. Am. Chem. Soc.* **1998**, *120*, 6761−6769.
(48) Söntjens, S. H. M.; Sijbesma, R. P.; van Genderen, M. H. P.; Meijer, E. W. Stability and Lifetime of Quadruply Hydrogen Bonded 2-Ureido-4[1H]-pyrimidinone Dimers. *J. Am. Chem. Soc.* **2000**, *122*, 7487−7493.
(49) Keizer, H. M.; Sijbesma, R. P.; Jansen, J. F. G. A.; Pasternack, G.; Meijer, E. W. Polymerization-Induced Phase Separation Using Hydrogen-Bonded Supramolecular Polymers. *Macromolecules* **2003**, *36*, 5602−5606.
(50) Dankers, P. Y. W.; van Leeuwen, E. N. M.; van Gemert, G. M. L.; Spiering, A. J. H.; Harmsen, M. C.; Brouwer, L. A.; Janssen, H. M.; Bosman, A. W.; van Luyn, M. J. A.; Meijer, E. W. Chemical and Biological Properties of Supramolecular Polymer Systems Based on Oligocaprolactones. *Biomaterials* **2006**, *27*, 5490−5501.
(51) Li, J.; Viveros, J. A.; Wrue, M. H.; Anthamatten, M. Shape-Memory Effects in Polymer Networks Containing Reversibly Associating Side-Groups. *Adv. Mater.* **2007**, *19*, 2851−2855.
(52) Guo, M.; Pitet, L. M.; Wyss, H. M.; Vos, M.; Dankers, P. Y. W.; Meijer, E. W. Tough Stimuli-Responsive Supramolecular Hydrogels with Hydrogen-Bonding Network Junctions. *J. Am. Chem. Soc.* **2014**, *136*, 6969−6977.
(53) Chen, X.; Dam, M. A.; Ono, K.; Mal, A.; Shen, H.; Nutt, S. R.; Sheran, K.; Wudl, F. A Thermally Re-mendable Cross-Linked Cross-Linked Polymeric Material. *Science* **2002**, *295*, 1698−1702.
(54) Klukovich, H. M.; Kean, Z. S.; Iacono, S. T.; Craig, S. L. Mechanically Induced Scission and Subsequent Thermal Remending of Perfluorocyclobutane Polymers. *J. Am. Chem. Soc.* **2011**, *133*, 17882−17888.
(55) Chung, C.-M.; Roh, Y.-S.; Cho, S.-Y.; Kim, J.-G. Crack Healing in Polymeric Materials via Photochemical [2 + 2] Cycloaddition. *Chem. Mater.* **2004**, *16*, 3982−3984.
(56) Ghosh, B.; Urban, M. W. Self-Repairing Oxetane-Substituted Chitosan Polyurethane Networks. *Science* **2009**, *323*, 1458−1460.
(57) Burattini, S.; Greenland, B. W.; Merino, D. H.; Weng, W.; Seppala, J.; Colquhoun, H. M.; Hayes, W.; Mackay, M. E.; Hamley, I. W.; Rowan, S. J. A Healable Supramolecular Polymer Blend Based on Aromatic π−π Stacking and Hydrogen-Bonding Interactions. *J. Am. Chem. Soc.* **2010**, *132*, 12051−12058.
(58) Hentschel, J.; Kushner, A. M.; Ziller, J.; Guan, Z. Self-Healing Supramolecular Block Copolymers. *Angew. Chem.* **2012**, *124*, 10713−10717.
(59) Chen, Y.; Kushner, A. M.; Williams, G. A.; Guan, Z. Multiphase Design of Autonomic Self-Healing Thermoplastic Elastomers. *Nat. Chem.* **2012**, *4*, 467−472.
(60) Luo, X.; Mather, P. T. Conductive Shape Memory Nanocomposites for High Speed Electrical Actuation. *Soft Matter* **2010**, *6*, 2146−2149.
(61) Huang, C.; Jiao, L.; Zhang, J.; Zeng, J.; Yang, K.; Wang, Y. Poly(butylene succinate)-poly(ethylene glycol) Multiblock Copolymer: Synthesis, Structure, Properties, and Shape Semory Performance. *Polym. Chem.* **2012**, *3*, 800−808.
(62) Botterhuis, N. E.; van Beek, D. J. M.; van Gemert, G. M. L.; Bosman, A. W.; Sijbesma, R. P. Self-Assembly and Morphology of Polydimethylsiloxane Supramolecular Thermoplastic Elastomers. *J. Polym. Sci., Part A: Polym. Chem.* **2008**, *46*, 3877−3885.
(63) Kim, B. K.; Lee, S. Y.; Xu, M. Polyurethanes Having Shape Memory Effects. *Polymer* **1996**, *37*, 5781−5793.

DOI: 10.1021/am507575z
ACS Appl. Mater. Interfaces 2015, 7, 2585−2596